International Journal of Fluid Machinery and Systems
Vol. 9, No. 1, January-March 2016

DOI: 10.5293/IJFMS.2016.9.1.057
ISSN (Online): 1882-9554

Original Paper

Numerical Analysis of Damping Effect of Liquid Film on Material in High Speed Liquid Droplet Impingement

Hirotoshi Sasaki[1], Naoya Ochiai[2] and Yuka Iga[2]

[1] Graduate School of Engineering, Tohoku University
6-6-01 Aramaki Aza Aoba Aoba-ku, Sendai 980-8579, Japan, hsasaki@cfs.ifs.tohoku.ac.jp
[2] Institute of Fluid Science, Tohoku University
2-1-1 Katahira Aoba-ku, Sendai 980-8577, Japan, ochiai@alba.ifs.tohoku.ac.jp, iga@cfs.ifs.tohoku.ac.jp

Abstract

By high speed Liquid Droplet Impingement (LDI) on material, fluid systems are seriously damaged, therefore, it is important for the solution of the erosion problem of fluid systems to consider the effect of material in LDI. In this study, by using an in-house fluid/material two-way coupled method which considers reflection and transmission of pressure, stress and velocity on the fluid/material interface, high-speed LDI on wet/dry material surface is simulated. As a result, in the case of LDI on wet surface, maximum equivalent stress are less than those of dry surface due to damping effect of liquid film. Empirical formula of the damping effect function is formulated with the fluid factors of LDI, which are impingement velocity, droplet diameter and thickness of liquid film on material surface.

Keywords: Liquid droplet, Liquid film, Fluid/material coupled numerical method, Homogeneous model, Elastic body material

1. Introduction

Serious damages are possibly caused by high speed droplet impingement on a material surface. In particular, wear of pipe material by liquid droplet impingement (LDI) erosion in piping system of nuclear power plant is becoming great problem in recent years because of high aging operation [1]. As respects the existing researches of LDI erosion, Heymann [2] showed that the erosion rate was proportion to 4.8th power of the droplet impingement velocity and 3.67th power of the droplet diameter. Sanchez [3] reported that the wear rate by droplet impingement is proportional to 4.0th power of V. In recent years, Hattori et al. [4] measured the relationship between the erosion rate and flow velocity of included droplet in the experiment of water jet, so that the erosion rate is proportional to 4.5~6.5th power of the flow velocity. Fujisawa et al. [5] showed that the erosion rate is proportional to 7th power of droplet impingement by experimental study with the high-speed conical spray-jet.

There are the various factors in LDI erosion. As for the influence of fluid factors, it is thought that the liquid thin film may exist on inner pipe surface because there may be humidity and repeated droplet impingement inside a steam pipe of an actual power plant. In addition, when the experimental method of water jet or spray is also used as the experiment of LDI, the liquid film seems to exist on material surface because of continuous droplet impingement. Fujisawa et al. [6] conducted an evaluation of effect of liquid film on material in LDI experimentally and suggested the equation of erosion rate considering the influence of liquid film.

In this study, by using an in-house fluid/material two way coupled method which considers reflection and transmission of pressure, stress and velocity on the fluid/material interface [7], high speed LDI on material surface is simulated. For the simulation of fluid, locally homogenous model of compressible gas-liquid two-phase medium is used for the simulation of liquid droplet in vapor. The governing equations of fluid-side are the 3D compressible gas-liquid two-phase Navier-Stokes equations. For the simulation of material, the governing equations composed of the equation of motion and the time-differential constitutive equations of homogeneous isotropic elastic medium are simultaneously solved. The material deformation and density change are neglected.

The algorithm of two-way coupled method at fluid/material interface is applied as follows: fluid pressure on material surface and normal stress of vertical direction of material surface are obtained by considering reflection and transmission of pressure, stress and velocity based on acoustic impedance. Nonslip condition is adopted on fluid/material surface, where the vertical velocity has the

Received November 27 2015; accepted for publication December 21 2016: Review conducted by Tadashi Tamura, Ph.D. (Paper number O15075S)
Corresponding author: Hirotoshi Sasaki, hsasaki@cfs.ifs.tohoku.ac.jp

This paper was presented at 13th Asian International Conference on Fluid Machinery (AICFM), September 7-10, 2015, Tokyo, Japan

values obtained by considering reflection and transmission and the tangential velocity of fluid has the same velocity of material which is calculated by material analysis. As for evaluation of stress in material, magnitude of stress in the material is evaluated by the von Mises's equivalent stress that is based on the concept of shear strain energy theory. From the numerical results, the relationship between maximum equivalent stress and variations of droplet diameter or impingement velocity in the LDI for wet surface have been estimated in order to obtain the knowledge of damping effect of liquid film on material surface in liquid droplet impingement. Additionally, by changing the liquid film thickness, the empirical formula of damping effect of liquid film is obtained against liquid film thickness, droplet diameter and impingement velocity.

2. Numerical Method

2.1 Governing Equations in Fluid

In this study, the locally homogeneous medium model of two-phase is used for the gas-liquid interface capture of droplet [8]. This locally homogeneous medium model is also used for the gas-liquid two-phase flow like cavitation flow [9]. The equation of state for a locally homogeneous gas-liquid two-phase medium is written as follows:

$$\rho = \frac{p\left(p + p_{\mathrm{c}}\right)}{K_{\mathrm{l}}\left(1-Y\right)p\left(T+T_0\right)+R_{\mathrm{g}}Y\left(p+p_{\mathrm{c}}\right)T}. \tag{1}$$

ρ is the mixture density and Y is the mass fraction of gas phase. p and T are respectively the pressure and the temperature which are assumed equilibrium between the gas phase and liquid phase. p_{c} and T_0 is the pressure and temperature constants of liquid respectively, R_{g} is the gas constant and K_{l} is the liquid constant. The total energy per unit volume of the gas-liquid two-phase medium e is written as follows:

$$\begin{aligned} &e = \rho C_{p\mathrm{m}} T + \rho h_{0\mathrm{m}} - p + \frac{1}{2}\rho\left|\vec{u}\right|^2. \\ &C_{p\mathrm{m}} = (1-Y)C_{p\mathrm{l}} + YC_{p\mathrm{g}}, \quad h_{0\mathrm{m}} = (1-Y)h_{0\mathrm{l}} + Yh_{0\mathrm{g}}. \end{aligned} \tag{2}$$

where C_{pm} is the specific heat at constant pressure of mixture and $h_{0\mathrm{m}}$ is the enthalpy constant of mixture.
The governing equations are the equation of continuity, the Navier-Stokes equations and the energy conservation equation for the compressible gas-liquid mixture phase flow, and the mass conservation equation of gas phase, which are expressed as follows:

$$\frac{\partial \boldsymbol{Q}}{\partial t} + \frac{\partial(\boldsymbol{E}-\boldsymbol{E}_{\mathrm{v}})}{\partial x} + \frac{\partial(\boldsymbol{F}-\boldsymbol{F}_{\mathrm{v}})}{\partial y} + \frac{\partial(\boldsymbol{G}-\boldsymbol{G}_{\mathrm{v}})}{\partial z} = \boldsymbol{S}_{\mathrm{m}} + \boldsymbol{S}_{\mathrm{sf}}. \tag{3}$$

$$\begin{aligned} &\boldsymbol{Q} = \left[\rho, \rho u, \rho v, \rho w, e, \rho Y\right]^t, \\ &\boldsymbol{E} = \left[\rho u, \rho u^2 + p, \rho uv, \rho uw, (e+p)u, \rho Y u\right]^t, \quad && \boldsymbol{E}_{\mathrm{v}} = \left[0, \tau_{xx}, \tau_{xy}, \tau_{xz}, \beta_x, 0\right]^t, \\ &\boldsymbol{F} = \left[\rho v, \rho vu, \rho v^2 + p, \rho vw, (e+p)v, \rho Y v\right]^t, && \boldsymbol{F}_{\mathrm{v}} = \left[0, \tau_{yx}, \tau_{yy}, \tau_{yz}, \beta_y, 0\right]^t, \\ &\boldsymbol{G} = \left[\rho w, \rho wu, \rho wv, \rho w^2 + p, (e+p)w, \rho Y w\right]^t, && \boldsymbol{G}_{\mathrm{v}} = \left[0, \tau_{zx}, \tau_{zy}, \tau_{zz}, \beta_y, 0\right]^t, \\ &\boldsymbol{S}_{\mathrm{m}} = [0,0,0,0,0,\dot{m}]^t, && \boldsymbol{S}_{\mathrm{sf}} = \left[0, -\kappa_{\mathrm{sf}}\sigma_{\mathrm{sf}}n_x, -\kappa_{\mathrm{sf}}\sigma_{\mathrm{sf}}n_y, -\kappa_{\mathrm{sf}}\sigma_{\mathrm{sf}}n_z, 0, 0\right]^t. \end{aligned} \tag{4}$$

where τ_{ij} and q_i are given by

$$\begin{aligned} &\tau_{ij} = \mu_{\mathrm{m}}\left(u_{i,j} + u_{j,i} - \frac{2}{3}\delta_{ij}u_{k,k}\right), \quad (i,j = x,y,z) \\ &\beta_i = -q_i + \tau_{ij}u_j, \quad q_i = -\kappa_{\mathrm{m}}T_i. \end{aligned} \tag{5}$$

β_i is the heat flux. The apparent viscosity coefficient μ_{m} and the mixture thermal conductance κ_{m} are defined as follows:

$$\begin{aligned} &\mu_{\mathrm{m}} = (1-\alpha)(1+2.5\alpha)\mu_{\mathrm{l}} + \alpha\mu_{\mathrm{g}}, \\ &\kappa_{\mathrm{m}} = (1-\alpha)\kappa_{\mathrm{l}} + \alpha\kappa_{\mathrm{g}}. \end{aligned} \tag{6}$$

The surface tension in source term $\boldsymbol{S}_{\mathrm{sf}}$ is calculated by using CFS model [10]. σ_{sf} is the surface tension constant, κ_{sf} is local surface curvature and n_x, n_y, n_z are the unit normal at the droplet interface.

Phase change model $\dot{m}$ in source term $\boldsymbol{S}_{\mathrm{m}}$ due to the evaporation and condensation is modeled by using the equation for vapor-liquid mixture [11] based on the theory of evaporation/condensation on a plane surface [12]

$$\dot{m} = \begin{cases} \dot{m}^+ & (p < p_{\mathrm{v}}) \\ \dot{m}^- & (p > p_{\mathrm{v}}) \end{cases}, \qquad \begin{aligned} &\dot{m}^+ = \frac{C_{\mathrm{c}}A\alpha(1-\alpha)}{\sqrt{2\pi R_{\mathrm{v}}T}}\left(\frac{\rho_{\mathrm{l}}}{\rho_{\mathrm{g}}}\right)(p_{\mathrm{v}} - p), \\ &\dot{m}^- = \frac{C_{\mathrm{c}}A\alpha(1-\alpha)}{\sqrt{2\pi R_{\mathrm{v}}T}}(p_{\mathrm{v}} - p), \end{aligned} \qquad A = C_a\alpha(1-\alpha). \tag{7}$$

where A is the interfacial area concentration in the vapor-liquid mixture and C_c is the evaporation/condensation coefficient. In this study, a value of C_cC_a=10000 is used. The saturated vapor pressure of water p_v is calculated by the empirical formula given by Sugawara [13].

2.2 Governing Equations in Material

For a simulation of stress wave propagation in material, it is assumed that material is elastic and the density ρ_s is nearly constant because the density change is very small in material. The following equation of motion and the time-differential constitutive equations of homogeneous isotropic elastic medium [14] are solved,

$$\frac{\partial \boldsymbol{Q}_s}{\partial t} = \frac{\partial \boldsymbol{E}_s}{\partial x} + \frac{\partial \boldsymbol{F}_s}{\partial y} + \frac{\partial \boldsymbol{G}_s}{\partial z}. \tag{8}$$

$$\begin{aligned}
\boldsymbol{Q}_s &= \left[\rho_s u_s, \rho_s v_s, \rho_s w_s, \sigma_{xx}, \sigma_{yy}, \sigma_{zz}, \sigma_{xy}, \sigma_{yz}, \sigma_{zx}\right]^t, \\
\boldsymbol{E}_s &= \left[\sigma_{xx}, \sigma_{xy}, \sigma_{xz}, \rho_s {c_1}^2 u_s, \rho_s {c_3}^2 u_s, \rho_s {c_3}^2 u_s, \rho_s {c_2}^2 v_s, 0, \rho_s {c_2}^2 w_s\right]^t, \\
\boldsymbol{F}_s &= \left[\sigma_{xy}, \sigma_{yy}, \sigma_{zy}, \rho_s {c_3}^2 v_s, \rho_s {c_1}^2 v_s, \rho_s {c_3}^2 v_s, \rho_s {c_2}^2 u_s, \rho_s {c_2}^2 w_s, 0\right]^t, \\
\boldsymbol{G}_s &= \left[\sigma_{zx}, \sigma_{zy}, \sigma_{zz}, \rho_s {c_3}^2 w_s, \rho_s {c_3}^2 w_s, \rho_s {c_1}^2 w_s, 0, \rho_s {c_2}^2 v_s, \rho_s {c_2}^2 u_s\right]^t.
\end{aligned} \tag{9}$$

$$c_1 = \sqrt{\frac{\lambda_s + 2\mu_s}{\rho_s}}, \quad c_2 = \sqrt{\frac{\mu_s}{\rho_s}}, \quad c_3 = \sqrt{\frac{\lambda_s}{\rho_s}}. \tag{10}$$

where λ_s and μ_s are Lame's constants, u_s, v_s, and w_s are displacement velocities of material. Then, the following relation holds between Young's modulus E and the Poisson ratio ν_s.

$$\lambda_s = \frac{\nu_s E}{(1+\nu_s)(1-2\nu_s)}, \quad \mu_s = \frac{E}{2(1+\nu_s)}. \tag{11}$$

2.3 Numerical Scheme

The cell centered finite volume formulation is used to discretize the governing equations in both fluid and material. The conservative variables are interpolated at the cell interfaces by using the 3rd-order MUSCL-TVD method with a minmod limiter. The 4th-order Runge-Kutta method is used for the time integration. The AUSM type scheme [15, 16] is used for the evaluation of numerical flux in the fluid side. In the material side, Godunov method [17] is used for upwind scheme.

2.4 Boundary between Fluid and Material

The algorithm of two-way coupled numerical method at fluid/material interface is applied as follows: fluid surface pressure and normal stress of vertical direction on material surface are obtained by considering reflection and transmission of pressure and stress waves with acoustic impedance [18]. Reflection and transmission rate of pressure waves and velocity incoming from the fluid side to the boundary of fluid/material are respectively R_{pf}, T_{pf}, R_{vf} and T_{vf}, on the other hand, from the material side to the boundary of fluid/material, these are respectively R_{ps}, T_{ps}, R_{vs} and T_{vs}. these are showed as follows:

$$R_{pf} = \frac{Z_s - Z_f}{Z_s + Z_f}, \qquad T_{pf} = \frac{2Z_s}{Z_s + Z_f}. \tag{12}$$

$$R_{vf} = \frac{-Z_s + Z_f}{Z_s + Z_f}, \qquad T_{vf} = \frac{2Z_f}{Z_s + Z_f}. \tag{13}$$

$$R_{ps} = \frac{Z_f - Z_s}{Z_s + Z_f}, \qquad T_{ps} = \frac{2Z_f}{Z_s + Z_f}. \tag{14}$$

$$R_{vs} = \frac{-Z_f + Z_s}{Z_s + Z_f}, \qquad T_{vs} = \frac{2Z_s}{Z_s + Z_f}. \tag{15}$$

Here, Z_f and Z_s are fluid and material acoustic impedance, which are given by the gas-liquid two-phase mixture density ρ and the fluid sound speed c, the material density ρ_s and the longitudinal sound speed of material c_1.

$$Z_f = \rho\, c\,, \quad Z_s = \rho_s c_1. \tag{16}$$

The pressure of fluid side virtual cell on the boundary of fluid/material p_{vc} is decided as follows:

$$p_{vc} = R_{pf}\, p_{wall} + T_{ps}(\sigma_{nn})_{wall}. \tag{17}$$

where p_{wall} is the pressure of the first cell from the boundary of fluid/material surface and $(\sigma_{nn})_{wall}$ is the normal stress of vertical direction of the first cell from the boundary surface.
The normal stress of vertical direction of material side virtual cell on the boundary of fluid/material $(\sigma_{nn})_{vc}$ is decided as follows:

$$(\sigma_{nn})_{vc} = T_{pf}\, p_{wall} + R_{ps}(\sigma_{nn})_{wall}. \tag{18}$$

Non-slip condition is adopted on fluid/material surface, where the vertical velocity has the values obtained by considering reflection and transmission. $(U_{fn})_{wall}$ is the vertical velocity of fluid side of the first cell on the boundary surface and $(\underline{U}_{sn})_{wall}$ is the vertical velocity of material side of the first cell on the boundary surface. Moreover, each velocity of virtual cell of $(U_{fn})_{vc}$ in the fluid side and $(U_{sn})_{vc}$ in the material side is decided as follows:

$$(U_{fn})_{vc} = R_{vf}(U_{fn})_{wall} + T_{vs}(U_{sn})_{wall}. \tag{19}$$

$$(U_{sn})_{vc} = T_{vf}(U_{fn})_{wall} + R_{vs}(U_{sn})_{wall}. \tag{20}$$

On the other hand, tangential velocity of fluid side has the same velocity of material surface which is calculated by analysis of material side. It corresponds to non-slip condition on material surface.

2.5 Calculation Condition

The initial temperature and pressure of water droplet in vapor are 293.15 K and 0.1 MPa respectively. The material phase is assumed to be carbon steel and the initial stress is compressive stress of 0.1 MPa. The material properties for carbon steel are set as follows: density ρ_s = 7800kg/m^3, Young's modulus E = 200 GPa and Poisson's ratio ν_s = 0.3. In the boundary of calculation domain, the temperature is fixed at 293.15 K.

In this calculation, because the displacement of material is very small in the occasion of micro scale single droplet impingement, the whole of material which includes material surface is calculated with fixed mesh system although the displacement velocity is taken into account. Due to assuming the phenomenon of plane symmetry, a quarter of all the space is calculated. The calculation grid is the 3-D orthogonal grid and the calculation area is 1.0d ×1.5d ×1.0d ((x direction) × (y direction) × (z direction)) in fluid side and 1.0d ×1.0d ×1.0d ((x direction) × (y direction) × (z direction)) in material side. The buffer area is placed in around the main calculation area. The grid numbers are 100 × 200 × 100 in fluid side and 100 × 100 × 100 in material side. Then, the grid spacing of horizontal direction on the material surface is equidistant grid spacing 0.01d in both fluid side and material side. For the grid spacing of vertical direction on the material surface, the calculation area of fluid side is the minimum grid spacing 0.0025d and the maximum grid spacing 0.02d and this grid spacing is gradually reduced as it approaches to the material boundary, and then the material side is equidistant grid spacing 0.01d. Moreover, the grid spacing of liquid film is equidistant grid spacing 0.0025d per a mesh toward the vertical direction on the material surface. Initial conditions of the calculation area is shown in Fig. 1.

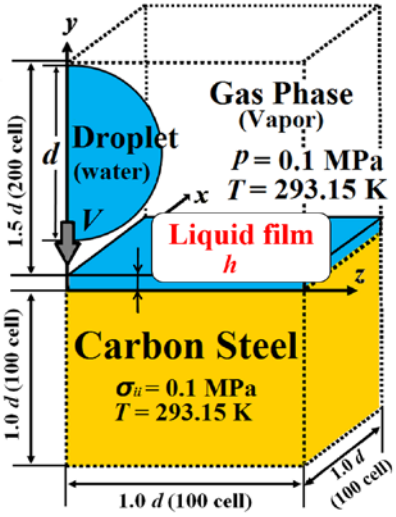

Fig.1 Initial condition of calculation area

2.6 The Evaluation of Equivalent Stress in the Material

Magnitude of stress in the material is evaluated by equivalent stress that is based on the concept of shear strain energy theory. The equivalent stress σ_{eq} is the von Mises's equivalent stress and written as follows:

$$\sigma_{eq} = \sqrt{\frac{(\sigma_{xx}-\sigma_{yy})^2 + (\sigma_{yy}-\sigma_{zz})^2 + (\sigma_{zz}-\sigma_{xx})^2}{2} + 3\left(\sigma_{xy}^2 + \sigma_{yz}^2 + \sigma_{zx}^2\right)}. \tag{21}$$

3. Results and Discussion

3.1 Feature of Droplet Impingement on Wet Surface

In order to know the effect of wetness on material surface on the impingement behavior and the distribution of pressure and equivalent stress in LDI, the 3-D simulation of vertical LDI on material surface with liquid film is performed and the result is compared with LDI on dry surface. In this calculation condition, liquid film thickness h is 0 and 5 μm, where film thickness of 0 μm means dry surface, impingement velocity V is 200 m/s, droplet diameter d is 0.1 mm. In the result, time t = 0 indicates the moment of impingement on wet or dry surface. Firstly, Fig. 2 shows the aspect of gas-liquid interface (void fraction α = 0.5) in case of impingement of dry surface and wet surface. When the droplet impinges on the dry surface, the side jet which flows on the material surface occurs, in the other hand, the splash occurs in the case of impingement on wet surface. Next, the time variations of the aspect of droplet impingement on dry and wet surface are shown in Figs. 3 and 4 respectively. In these figures, gas-liquid interface of droplet is drawn by black solid line which is assumed at void fraction 0.5. In the case of LDI on dry surface, the high equivalent stress occurs at impingement center just after impingement and contact edge which is formed at droplet and material surface after impingement. On the other hand, in the case of LDI on wet surface, the impinged pressure is absorbed in droplet inner and liquid film, and then the pressure of contact edge is also absorbed by fluid-fluid contact. Because these pressures reach material surface after propagating liquid film, the equivalent stress is considerably decreased.

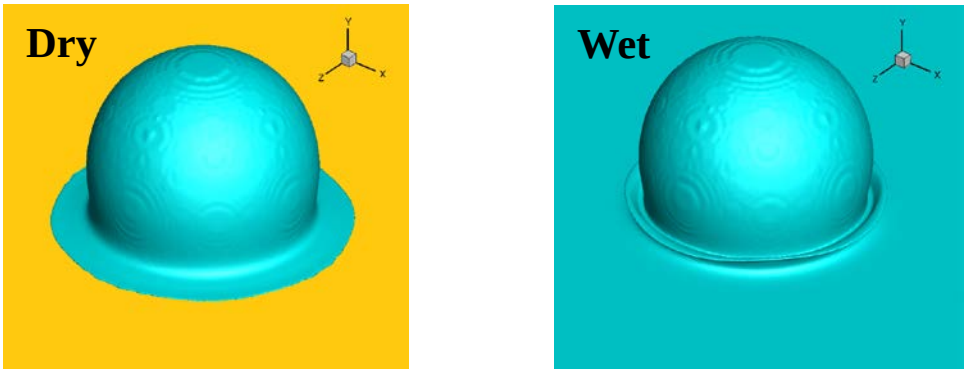

Fig. 2 Aspect of gas-liquid interface in case of impingement of dry and wet surface (d = 0.1mm, V = 200 m/s, h =5 μm)

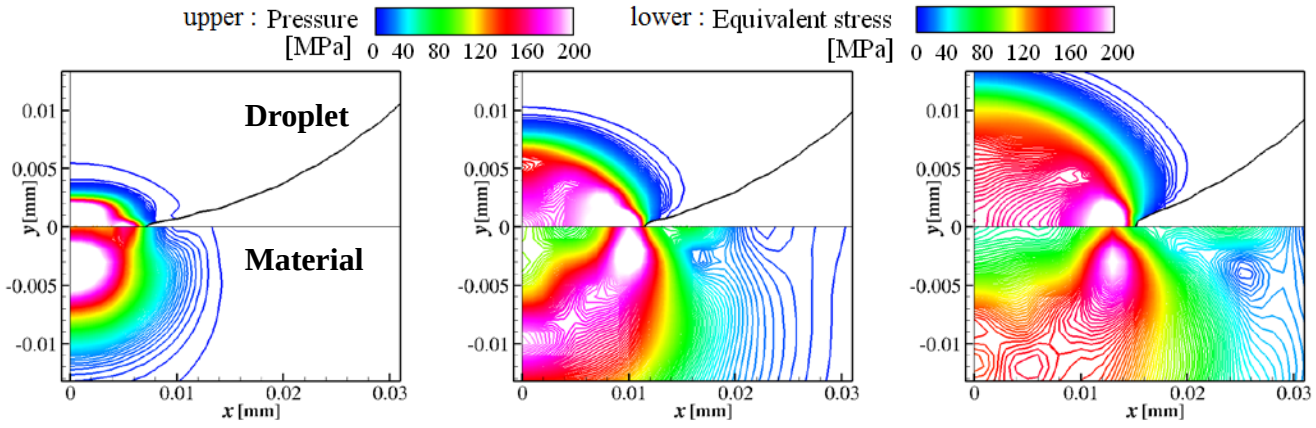

(a) t = 0.002 μs (b) t = 0.006 μs (c) t = 0.009 μs

Fig. 3 Time variation of pressure in fluid and equivalent stress in material on dry surface (d = 0.1mm, V = 200 m/s)

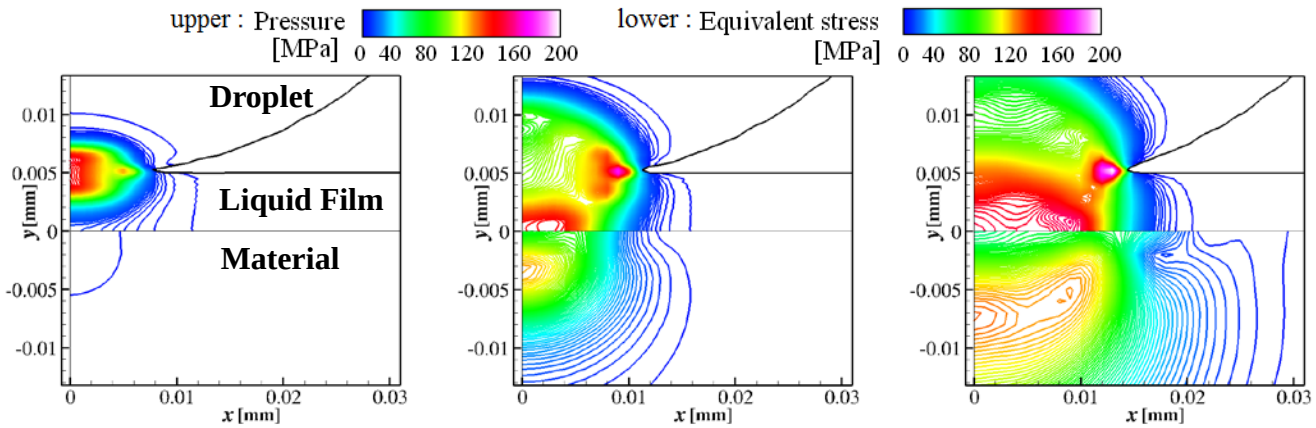

(a) t = 0.003 μs (b) t = 0.006 μs (c) t = 0.009 μs

Fig. 4 Time variation of pressure in fluid and equivalent stress in material on wet surface (d = 0.1mm, V = 200 m/s, h = 5 μm)

In addition, Fig.5 shows the flow velocity vector around droplet and liquid film. These figures show that liquid film is lifted in the contact edge of the droplet and becomes splash by droplet impingement on liquid film. Then, the part of kinetic energy of droplet is transformed to potential energy and also to kinetic energy of liquid film. This phenomena causes the decrement of impingement energy of the droplet. Figure 6 shows the distribution of maximum pressure of fluid side p_{max} and maximum equivalent stress of material side $(\sigma_{eq})_{max}$ in each cell on wet surface and dry surface. As mentioned before in the time evaluation in each impingement, this figure also shows that $(\sigma_{eq})_{max}$ inside the material is drastically decreased by wetness on material surface.

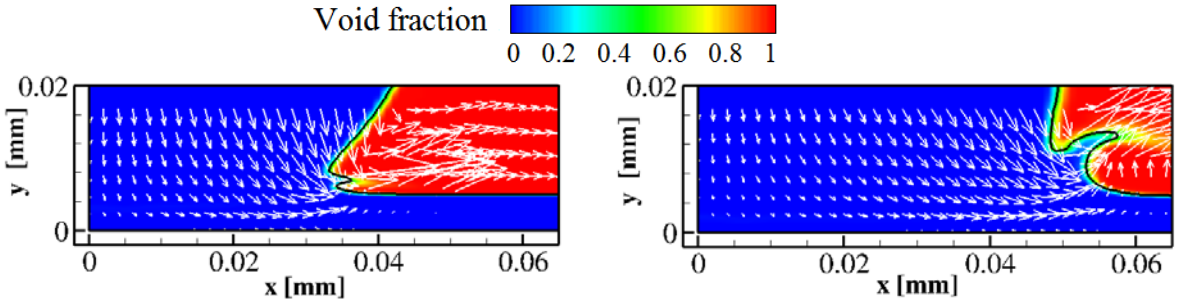

(a) t = 0.040 μs (b) t = 0.100 μs

Fig. 5 Distribution of the flow velocity vector around droplet and liquid film (d = 0.1mm, V = 200 m/s, h =5 μm)

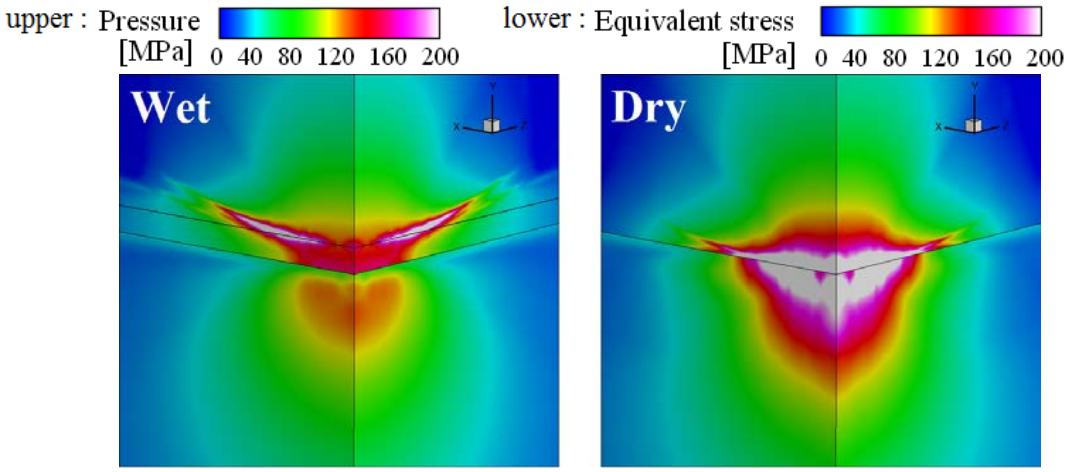

Fig. 6 Comparison of distribution of maximum pressure and maximum equivalent stress in each cell (d = 0.1mm, V = 200 m/s, h =5 μm)

3.2 Damping Effect of Liquid Film on Maximum Equivalent Stress

Numerical analysis with changing of the liquid film thickness is conducted in order to estimate the damping effect. The result of maximum equivalent stress $(\sigma_{eq})_{max}$ by relationship between film thickness h and droplet diameter d is shown in Table 1. This table shows that $(\sigma_{eq})_{max}$ depends on the ratio of h and d when impingement velocity V is constant (V = 200 m/s). For example, when h/d is 0.05, $(\sigma_{eq})_{max}$ is 123 MPa. In other cases, if h/d is the same value, $(\sigma_{eq})_{max}$ is also almost the same value.

Table 1 Resulting $(\sigma_{eq})_{max}$ in variation of h and d (V = 200 m/s)

h [μm] / d [mm]	0(dry)	2.5	5.0	10
0.05	**273 [**MPa]	**123**	**88**	**56**
0.1	**274**	**171**	**123**	**88**
0.2	**275**	**208**	**170**	**123**
0.5	**276**	**243**	**220**	**186**
1.0	**276**	**251**	**243**	**221**

These results are summarized in Fig. 7, which is the relationship between the ratio of h and d and the impingement damping coefficient η. The impingement damping coefficient η is defined as follows in this study:

$$\eta = (\sigma_{eq\_wet})_{max} / (\sigma_{eq\_dry})_{max} . \tag{22}$$

In Fig. 7, the blue triangle shows the result of d = 0.05 mm, the red circle shows the result of d = 0.1 mm, the green square shows the d = 0.2 mm, the purple inverted triangle is the d = 0.5 mm and the magenta diamond shape is the d = 1.0 mm and the red solid line is the fitting curve. According to Fig. 7, when V is constant (V = 200 m/s), the relationship between η and h/d can be expressed by an exponential decay function. This function is shown as eq. (23) and then these fitting parameters a and b are respectively a = 3.5 and b = 0.5.

$$\eta = \exp\left(-a\left(\frac{h}{d}\right)^{b}\right). \tag{23}$$

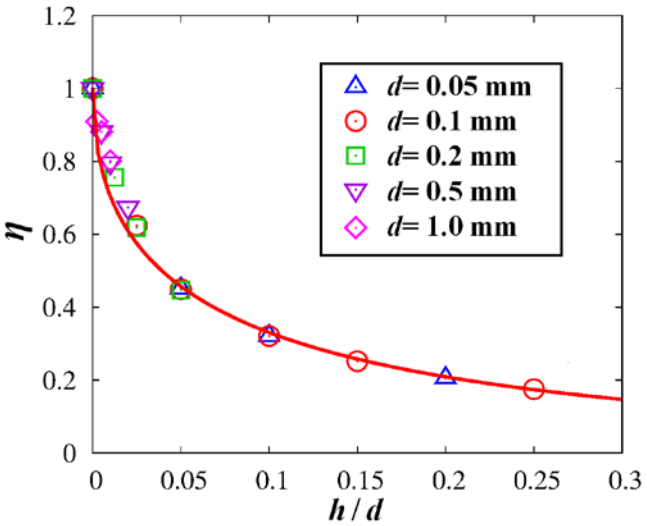

Fig. 7 Relationship between η and h/d (V = 200 m/s)

Next, Fig. 8 shows the relationship between η and h/d in the case of changing impingement velocity V. As V becomes high, η also becomes large, which means that the increment of V leads to the decrement of the impingement damping effect of $(\sigma_{eq})_{max}$. Even if V changes, the relation of η and h/d can be shown by the same exponential decay function of eq. (23). In this case, the function parameter of a is changed by variation of V but b is constant regardless of V. These parameters are summarized in Table 2.

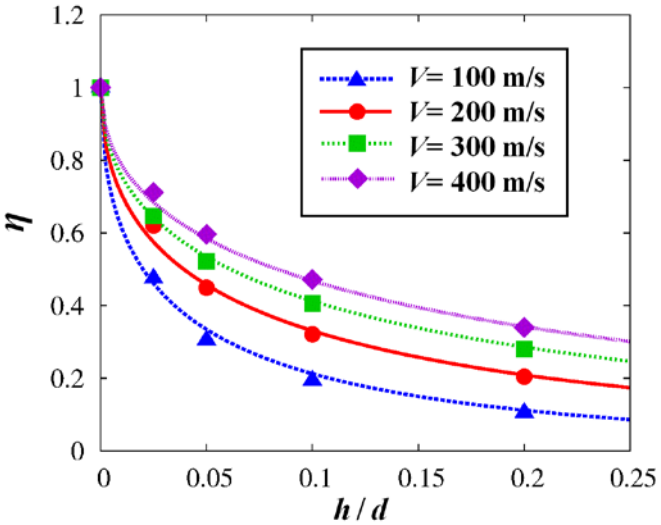

Fig. 8 Relationship between η and h/d with variation of V (d = 0.1 mm)

Table 2 Parameter of a and b in function η with variation of V

V [m/s]	a	b
100	**4.9**	**0.5**
200	**3.5**	**0.5**
300	**2.8**	**0.5**
400	**2.4**	**0.5**

Based on the result, it is thought that the parameter of a is the function of V. The relationship between a and V is shown in Fig. 9. The parameter of a can be expressed by the exponential function of V.

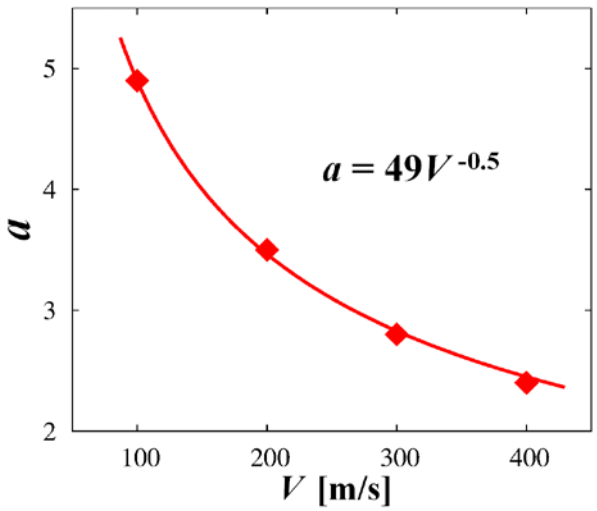

Fig. 9 Relationship between a and V (d = 0.1 mm)

$$a = 49V^{-0.5}. \tag{24}$$

Then, eq. (23) and (24) can be summarized in a single function of eq. (25). Therefore, the function of impingement damping coefficient of η can be expressed by the relation of film thickness h, droplet diameter d and impingement velocity V, which are fluid factors in LDI.

$$\eta = \exp\left(-49\left(\frac{h}{Vd}\right)^{0.5}\right). \tag{25}$$

4. Conclusion

The simulations of vertical droplet impingement on a dry and wet material surface were carried out by using our in-house fluid/material coupled numerical method which considers reflection and transmission of waves on the fluid/material interface. The obtained results can be summarized as follows:

(1) In the case of LDI on wet surface, it is shown that the impinged pressure of droplet is decreased because the impinged energy is deprived by the occurrence of splash and the flow inside liquid film. Moreover, because the pressure waves decay during propagation inside liquid film, the equivalent stress inside material generated by the pressure wave is drastically decreased compared with that in dry surface.

(2) The maximum equivalent stress takes constant value in the condition in which the ratio of liquid film thickness and droplet diameter is constant.

(3) The damping effect of liquid film on maximum equivalent stress depends on the various fluid factors and the empirical formula of the damping function is derived from the exponential decay function of a single relation composed by liquid film thickness, droplet diameter and impingement velocity.

Nomenclature

c	sound speed of fluid [m/s]	Y	mass fraction of gas phase [-]
c_1	sound speed of material [m/s]	Z	acoustic impedance [Pa・ s/m]
d	droplet diameter [mm]	α	void fraction [-]
e	total energy per unit volume [J/m^3]	η	impingement damping coefficient [-]
E	Young's modulus [GPa]	μ_s, λ_s	Lame's constant [GPa]
h	film thickness [μm]	ν_s	Poisson's ratio [-]
p	pressure [MPa]	ρ	fluid density [kg/m^3]
t	time [μs]	ρ_s	material density [kg/m^3]
T	temperature [K]	σ_{eq}	equivalent stress [MPa]
V	droplet impingement velocity [m/s]		

References

[1] Press release of Tohoku Electric Power, 2007, “Investigation and Preventive Steps of Vent Piping System Feedwater Heater 2 of Onagawa Nuclear Power Station Unit 2, Dec. 12th, (in Japanese).
[2] Heymann, F. J., 1979, “Conclusions from the ASTM interlaboratory test program with liquid impact erosion facilities”, Proc. 5th Int. Conf. on Erosion by Liquid and Solid Impact, pp. 20-1–20-10.
[3] Sanchez-Caldera, L. E., 1984, “The Mechanism of Corrosion-Erosion in Steam Extraction Lines of Power Stations”, Ph. D. Thesis. Dep. Mech. Eng., Massachusetts Institute of Technology.
[4] Hattori, S., Hayakawa, H. and Takinami, M., 2008, “Liquid Impingement Erosion of Steels”, Proc. 13th Forefront of Power and Energy Systems Symposium, JSME, pp. 37-40 (in Japanese).
[5] Fujisawa, N., Yamagata, T., Hayashi, K. and Takano, T., 2012, “Experiments on Liquid Droplet Impingement Erosion by High-Speed Spray”, Nucl. Eng. Des., Vol. 250, pp. 101-107.
[6] Fujisawa, N., Yamagata, T., Saito, K. and Hayashi, K., 2013, “The effect of liquid film on liquid droplet impingement erosion”, Nucl. Eng. Des., Vol. 265, pp. 909-917.
[7] Sasaki, H., Iga, Y., and Ikohagi, T., 2010, “Study of Droplet Impingement Phenomena by Fluid/Solid Coupled Simulation”, Proc. Joint Int. Conf. on Supercomputing in Nuclear Applications and Monte Carlo 2010, Paper No. 10189.
[8] Okuda, K. and Ikohagi, T., 1996, “Numerical Simulation of Collapsing Behavior of Bubble Clouds”, Trans. JSME, Ser. B., Vol. 62 (603), pp. 3792–3797 (in Japanese).
[9] Iga, Y. and Konno, T., 2012, “Numerical Analysis of the Influence of Acceleration on Cavitation Instabilities that arise in Cascade”, International Journal of Fluid Machinery and Systems, Vol. 5, No. 1 (January - March), pp. 1-9.
[10] Brackball, J. U., Kothe, D. B. and Zemach, C., 1992, “A Continuum Method for Modeling Surface Tension”, J. Comp. Phys., Vol. 100 (2), pp. 335-354.
[11] Nakamori, I. and Ikohagi, T., 2002, “Numerical Method for Cavitating Flow with Phase Change”, Proc. 5th JSME/KSME Fluids Eng. Conf., Paper No. 322.
[12] Fujikawa, S., and Akamatsu, T., 1980, “Effects of the Non-equilibrium Condensation of Vapor on the Pressure Wave Produced by the Collapse of a Bubble in a Liquid”, J. Fluid Mech., Vol. 97, pp. 481-512.
[13] Sugawara, S., 1932, “New Steam Tables”, JSME, Vol. 35 (186), pp. 999-1004, (in Japanese).
[14] Takano, Y., Goto, T. and Nishino, S., 1998, “A Finite Volume Scheme for Elastodynamic Equations (1st Report, Algorithm for Elastodynamics)”, JSME. Ser. A., Vol. 64 (626), pp. 2471-2476 (in Japanese).
[15] Shima, E. and Jounouchi, T., 1994, “Role of Computational Fluid Dynamics in Aeronautical Engineering (No.12) - Formulation and Verification of Uni - Particle Upwind Schemes for the Euler Equations -”, NAL-SP27, Proc. 12th NAL Symp. on Aircraft Computational Aerodynamics, pp. 255-260.
[16] Edwards, J. R., Franklin, R. and Liou, M., 2000, “Low-Diffusion Flux-Splitting Methods for Real Fluid Flows with Phase Transitions”, AIAA J., Vol. 38 (9), 1624-1633.
[17] Godunov, S. K., 1959, “A Difference Method for Numerical Calculation of Discontinuous Solutions of the Equations of Hydrodynamics”, Matematicheskii Sbornik, Vol. 47 (89), No. 3, pp. 271-306.
[18] Yasuda, K., 2004, “Mechanical Acoustics”, CORONA PUBLISHING CO., LTD., Tokyo (in Japanese).